PET/CT Motion Correction Exploiting Motion Models Fit on Coarsely Gated Data Applied to Finely Gated Data

Alexander C. Whitehead *Student Member, IEEE*, Kuan-Hao Su,
Scott D. Wollenweber *Senior Member IEEE*, Jamie R. McClelland and
Kris Thielemans *Senior Member, IEEE*

Abstract—Motion correction is imperative to the reduction of blurring and artefacts inherent in PET; due to the relatively long acquisition time, and the temporal difference in the attenuation map acquisition. Registration literature contains many examples of spatial regularisers, however there are few temporal regularisers. Motion models can act as such a temporal regulariser, as well as allowing for the interpolation of unseen motion correction results. In our previous work, we applied a motion modelling approach to high TOF resolution non-attenuation corrected data; where the data was corrected to the space of the attenuation map. However, this approach was challenging, especially when low contrast lung tumours are present. This work seeks to extend previous work, by incorporating an approach suggested by Y. Lu et al. (JNM 2018), to perform an initial MLACF reconstruction for the motion estimation. In this work, we combine these two approaches, with several improvements, including; μ-map alignment, as well as, fitting the motion model on low noise low temporal/gate resolution data, and applying it to high noise high temporal/gate resolution data. To test this, XCAT volumes are constructed, and TOF data simulated. Evaluation compares the results of the proposed method against, where the motion model was fit on data gated more finely, where the motion model was fit on noiseless data, and finally non-motion corrected examples. Results indicate that the incorporation of MLACF, and fitting of the motion model on low noise low temporal/gate resolution data, improves contrast and quantification, while allowing for a relatively fast execution time.

I. INTRODUCTION

MOTION Models parameterise Deformation Vector Fields (DVFs) in terms of a Surrogate Signal (SS). They could be considered as an addition to a standard spatially regularised Motion Correction (MC) technique, as they impose a degree of temporal or gate-wise regularisation. In addition, they also allow obtaining DVFs for time points/gates, not used to fit the model (as long as a relevant SS exists [1]). Motion Models (MMs) have seen attention, particularly in CT [2], but also MR [3], [4], however less so in clinical PET/CT.

In our previous work [5]–[7], the possibility of incorporating MMs, in a MC framework, for Non-Attenuation Corrected (NAC) Time-of-Flight (TOF) PET, where the reference was set to the position of a breath hold Attenuation Map (Mu-Map), was investigated. Our preliminary experiments indicated that the combination of both the MM and TOF, allowed for an Attenuation Corrected (AC) reconstruction with MC, without introducing artefacts, while increasing resolution and quantification accuracy (for simulations with high TOF resolution and count levels). This work seeks to extend the method further, using more realistic simulation and count levels, from existing clinical scanners. Firstly, by incorporating MLACF , which provides volumes with greater contrast than NAC, without introducing bias due to misalignment with a fixed Mu-Map [8]. Secondly, low noise low temporal/gate resolution data is used to fit the MM, while high noise high temporal/gate resolution data is used for the output;

this potentially allows for reduced misregistration, as well as improving computation time. Thirdly, a diffeomorphic velocity field parameterised registration was used ,which provided DVFs free from folding.

A method incorporating MMs for dynamic PET/CT, was proposed in [9]. Additionally, a method incorporating MLACF for PET/CT, was proposed in [10]. The work presented here, differentiates itself, not only by the ways mentioned above, but also by using a 2D SS (rather than a 1D SS). Thus allowing more general parametrisation of the motion (here in terms of both displacement and velocity). Additionally, the group-wise method, presented here, makes use of an iterative MC algorithm, rather than relying only on a pair-wise method.

II. METHODS

A. XCAT Volume Generation

XCAT [11] was used to generate 480 volumes over a 240 s period, using respiratory traces, derived from 2D CINE-MR patient data. The maximum displacement of Anterior Posterior (AP) and Superior Inferior (SI) motion, was set to 1.2 cm and 2.0 cm respectively. Activity concentrations were derived from a static 18F-FDG patient scan. The Field of View included the base of the lungs, diaphragm, and the top of the liver, with a 20 mm diameter spherical lesion placed into the base of the right lung (within the maximum displacement due to Respiratory Motion of the diaphragm).

B. PET Acquisition Simulation

PET acquisitions were simulated (and reconstructed), using STIR [12], [13] through SIRF [14], to forward project data using the geometry of a GE Discovery 710. Attenuation was included using the relevant Mu-Maps generated by XCAT. Pseudo-randoms and scatter were added.

Noise was simulated, such that data matched an acquisition over 240 s, emulating a standard single bed position acquisition. The count rate was selected to match that of research scans.

A respiratory SS was generated using Principal Component Analysis (PCA) [15]. The value of this signal, and its gradient, was used for gating. For MM estimation, data were initially pseudo-phase gated; the data was displacement and gradient gated into four bins, where each bin was a quadrant centred on the maximum or minimum of the displacement or gradient. For the purpose of the MM fitting, SS values were determined for the post-gated data by taking an average of the SS values in each bin.

C. MLACF Image Reconstruction

Data were reconstructed using MLACF, with seven full iterations and 24 subsets for the activity update, and nine iterations for the attenuation update [8]. MLACF was initialised using one iteration of MLEM, where the breath hold CT was used for AC. Between iterations, the activity volume and Attenuation Correction Factors (ACF) sinogram were normalised (scaled to the same magnitude as an equivalent volume/sinogram filled with ones), and a small value was added to each voxel. A quadratic prior was included in the reconstruction, to promote smoothness of the ACF sinogram.

D. Registration

Before being registered, each volume underwent preprocessing, including; replication of end-slices, smoothing, and standardisation. This pre-processing was only applied to intermediate data, and was not used for the final output of the method.

Group-wise registration was used, where after an initial pair-wise registration step, a new reference volume was resampled. Registration to the new reference volume, followed by another resample, continued for a set number of iterations. NiftyReg [16] was used to perform registrations, using a diffeomorphic velocity field B-spline parameterisation. Control Point Grid spacing of the B-spline coefficients, Bending Energy regularisation term weight, and number of iterations were tuned using a grid search.

Between each iteration, the resampled volume was registered to the position of the Mu-Map. The DVFs for both the group-wise registration, and Mu-Map registration were composed together to form one final DVF.

E. Motion Model Estimation

MMs were fit as a direct Respiratory Correspondence Model on the Control Point Grids (CPGs), and the SS. A weighted Linear Regression was used, where the weighting was taken based on the number of counts in each gate. Once a MM was fit, new DVFs were generated for each gate. MM fitting occurred between iterations.

F. MC Image Reconstruction with AC

Data were re-gated, using the value of SS, and its gradient, to gate data into 30 respiratory bins (10 displacement and 3 gradient bins).

Data were re-reconstructed with AC, deforming the Mu-Maps, using the inverse of the DVFs determined using the MM. OSEM was used, with two full iterations and 24 subsets (as in clinical practice) [17]. MC was then
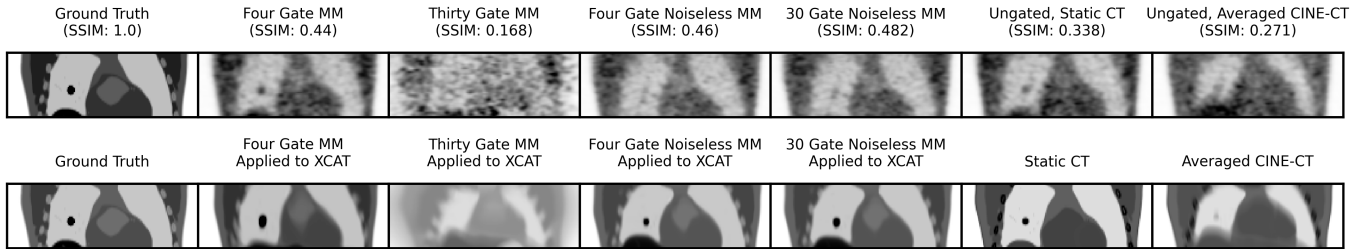
Fig. 1. First row contains, AC MC reconstructions (plus SSIM to the ground truth), and the second row contains, the results of applying the final MM on the original XCAT volumes, with the ground truth XCAT data (for both activity and attenuation), for; a MM fit on four and 30 gate binned data applied to 30 gate binned data, a MM fit on noiseless four and 30 gate binned data applied to 30 gate binned data, and ungated data AC with a static Mu-Map at end inhalation and all Mu-Maps summed. Colour map ranges are consistent for all images in each row.

applied, using DVFs determined using the MM. Volumes were post-filtered using a Gaussian smoothing, with a FWHM of $6.4 \, \text{mm}$ in the transverse plane, and a normal Z-filter (as in clinical practice).

G. Evaluation

In addition to the reconstructions performed above, MC was also applied to data in the same way, but using high noise, high temporal/gate resolution, or noiseless data, for the MM fitting. Furthermore, data were also reconstructed without MC, using either the end inhalation Mu-Map, or a sum of all Mu-Maps (to emulate an Averaged CINE-CT (AV-CCT)). For the present evaluation, the volumes without MC were registered to the position of the end inhalation Mu-Map. Additionally, DVFs generated by each method were also applied to the original XCAT volumes, for visual analysis.

Comparisons used included: A visual analysis, SSIM to the ground truth [18], a profile over the lesion, and SUV_{max} and SUV_{peak} (defined following EANM guidelines [19]).

III. RESULTS

A visual comparison of the reconstructed images (see Fig. 1), shows that the high noise high temporal/gate resolution method performs quite poorly, most probably due to the high level of noise apparent in the volumes. Conversely, the low noise low temporal/gate resolution data method appears to be able to MC the data without being too adversely affected by the noise level.

The peak of the profile (see Fig. 2) for the four gate MM results is comparable to the noiseless results. In contrast, the 30 gate MM method fails on the noisy data. For all other MC methods, the peak is greater than without MC.

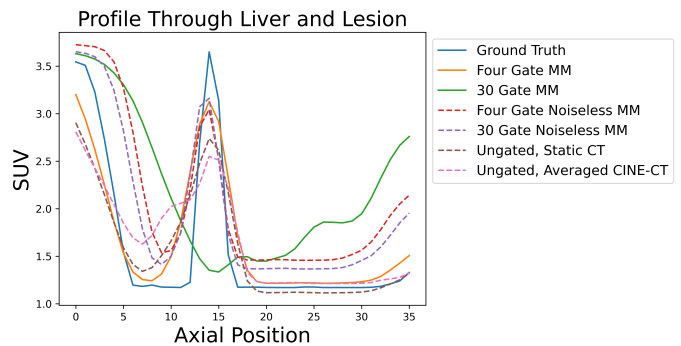SUV (and SSIM) results confirm the above (see TABLE I).

Fig. 2. A profile through the lesion, in the SI direction, summed over a window in the AP and Lateral Medial directions, with median smoothing, for; the ground truth XCAT data, a MM fit on four and 30 gate binned data applied to 30 gate binned data, a MM fit on noiseless four and 30 gate binned data applied to 30 gate binned data, and ungated data AC with a static Mu-Map at end inhalation and all Mu-Maps summed.

TABLE I

COMPARISON OF SUV_{MAX} AND SUV_{PEAK}, FOR; THE GROUND TRUTH XCAT DATA, A MM FIT ON FOUR AND 30 GATE BINNED DATA APPLIED TO 30 GATE BINNED DATA, A MM FIT ON NOISELESS FOUR AND 30 GATE BINNED DATA APPLIED TO 30 GATE BINNED DATA, AND UNGATED DATA AC WITH A STATIC MU-MAP AT END INHALATION AND ALL MU-MAPS SUMMED.

SUV	Max	Peak
Ground Truth	8.76	7.96
Four Gate MM	8.04	6.18
30 Gate MM	1.77	1.32
Four Gate Noiseless MM	8.05	6.24
30 Gate Noiseless MM	7.96	5.99
Ungated, Static CT	6.61	5.08
Ungated, AV-CCT	5.65	4.44

IV. DISCUSSION AND CONCLUSIONS

Results show that using a low number of gates for MM fitting, has minimal impact at low noise, while improving MC when there is a high level of noise in the gates. In addition, the execution time using a reduced number of gates is lower.

In the future, work will focus on evaluating the method on patient data.

REFERENCES

[1] J. R. McClelland *et al.*, "Respiratory motion models: A review," *Medical Image Analysis*, vol. 17, no. 1, pp. 19–42, Jan. 2013.

[2] T. Li *et al.*, "Enhanced 4D cone-beam CT with inter-phase motion model," *Medical Physics*, vol. 34, no. 9, pp. 3688–3695, Aug. 2007.

[3] D. Manke *et al.*, "Respiratory motion in coronary magnetic resonance angiography: A comparison of different motion models," *Journal of Magnetic Resonance Imaging*, vol. 15, no. 6, pp. 661–671, Jun. 2002.

[4] R. Manber *et al.*, "Joint PET-MR respiratory motion models for clinical PET motion correction.," *Physics in medicine and biology*, vol. 61, no. 17, pp. 6515–30, Sep. 2016.

[5] A. C. Whitehead *et al.*, "Impact of Time-of-Flight on Respiratory Motion Modelling using Non-Attenuation-Corrected PET," in *IEEE NSS-MIC*, IEEE, Oct. 2019.

[6] A. C. Whitehead *et al.*, "PET/CT Respiratory Motion Correction With a Single Attenuation Map Using NAC Derived Deformation Fields," in *IEEE NSS-MIC*, IEEE, Aug. 2020, pp. 1–3.

[7] A. C. Whitehead *et al.*, "Comparison of Motion Correction Methods Incorporating Motion Modelling for PET/CT Using a Single Breath Hold Attenuation Map," in *IEEE NSS-MIC*, IEEE, Sep. 2021, pp. 1–4.

[8] J. Nuyts *et al.*, "ML-reconstruction for TOF-PET with simultaneous estimation of the attenuation factors," *IEEE NSS-MIC, IEEE*, pp. 2147–2149, 2012.

[9] C. Chan *et al.*, "Non-Rigid Event-by-Event Continuous Respiratory Motion Compensated List-Mode Reconstruction for PET," *IEEE Transactions on Medical Imaging*, vol. 37, no. 2, pp. 504–515, Feb. 2018.

[10] Y. Lu *et al.*, "Respiratory Motion Compensation for PET/CT with Motion Information Derived from Matched Attenuation-Corrected Gated PET Data," *Journal of Nuclear Medicine*, vol. 59, no. 9, pp. 1480–1486, Sep. 2018.

[11] W. P. Segars *et al.*, "4D XCAT phantom for multimodality imaging research," *Medical Physics*, vol. 37, no. 9, pp. 4902–4915, Aug. 2010.

[12] K. Thielemans *et al.*, "STIR: software for tomographic image reconstruction release 2," *Physics in Medicine and Biology*, vol. 57, no. 4, pp. 867–883, Feb. 2012.

[13] N. Efthimiou *et al.*, "Implementation and validation of time-of-flight PET image reconstruction module for listmode and sinogram projection data in the STIR library," *Physics in Medicine and Biology*, vol. 64, no. 3, p. 035 004, Jan. 2019.

[14] E. Ovtchinnikov *et al.*, "SIRF: Synergistic Image Reconstruction Framework," in *IEEE NSS-MIC*, IEEE, Oct. 2017, pp. 1–3.

[15] K. Thielemans *et al.*, "Device-less gating for PET/CT using PCA," in *IEEE NSS-MIC*, IEEE, 2011.

[16] M. Modat *et al.*, "Fast free-form deformation using graphics processing units," *Computer Methods and Programs in Biomedicine*, vol. 98, no. 3, pp. 278–284, 2010.

[17] H. M. Hudson *et al.*, "Accelerated Image Reconstruction Using Ordered Subsets of Projection Data," *IEEE Transactions on Medical Imaging*, vol. 13, no. 4, pp. 601–609, 1994.

[18] Z. Wang *et al.*, "Mean squared error: Lot it or leave it? A new look at signal fidelity measures," *IEEE Signal Processing Magazine*, vol. 26, no. 1, pp. 98–117, 2009.

[19] R. Boellaard *et al.*, "FDG PET/CT: EANM procedure guidelines for tumour imaging: version 2.0," *European Journal of Nuclear Medicine and Molecular Imaging*, vol. 42, no. 2, pp. 328–354, 2015.